Biochimica et Biophysica Acta 1848 (2015) 115–126

Contents lists available at ScienceDirect

Biochimica et Biophysica Acta

journal homepage: www.elsevier.com/locate/bbamem

Assembly of streptolysin O pores assessed by quartz crystal microbalance and atomic force microscopy provides evidence for the formation of anchored but incomplete oligomers

Sarah E. Stewart [a], Michael E. D'Angelo [a], Stefania Piantavigna [b], Rico F. Tabor [b], Lisandra L. Martin [b], Phillip I. Bird [a,*]

[a] Department of Biochemistry and Molecular Biology, Monash University, Clayton, Australia
[b] School of Chemistry, Monash University, Clayton, Australia

ARTICLE INFO

Article history:
Received 25 June 2014
Received in revised form 20 September 2014
Accepted 3 October 2014
Available online 12 October 2014

Keywords:
Streptolysin O
Pore
Quartz crystal microbalance
Bacterial toxin
Atomic force microscopy
Cholesterol dependent cytolysin

ABSTRACT

Streptolysin O (SLO) is a bacterial pore forming protein that is part of the cholesterol dependent cytolysin (CDC) family. We have used quartz crystal microbalance with dissipation monitoring (QCM-D) to examine SLO membrane binding and pore formation. In this system, SLO binds tightly to cholesterol-containing membranes, and assembles into partial and complete pores confirmed by atomic force microscopy. SLO binds to the lipid bilayer at a single rate consistent with the Langmuir isotherm model of adsorption. Changes in dissipation illustrate that SLO alters the viscoelastic properties of the bilayer during pore formation, but there is no loss of material from the bilayer as reported for small membrane-penetrating peptides. SLO mutants were used to further dissect the assembly and insertion processes by QCM-D. This shows the signature of SLO in QCM-D changes when pore formation is inhibited, and that bound and inserted SLO forms can be distinguished. Furthermore a pre-pore locked SLO mutant binds reversibly to lipid, suggesting that the partially complete wtSLO forms observed by AFM are anchored to the membrane.

1. Introduction

Pore forming toxins are produced by a variety of organisms. These include the cholesterol dependent cytolysin (CDC) family of virulence factors from Gram-positive bacteria. CDCs are released as monomers which interact with the host cell membrane and oligomerise to form large aqueous pores, reviewed in detail [1]. The current model for pore formation suggests that soluble CDC monomers bind to the membrane via cholesterol [2,3], initiating a change in conformation that allows membrane bound monomer–monomer binding [4–6]. The monomers oligomerise until a ring structure is completed, which is termed the pre-pore complex. The pre-pore complex subsequently undergoes conformational change involving concerted vertical collapse as each monomer unravels two α-helical bundles to form two β-hairpins that penetrate the membrane. This creates a large β-barrel pore [7–9].

Streptolysin O (SLO) is a CDC expressed by *Streptococcus pyogenes*. SLO is required to translocate nicotinamide adenine dinucleotide (NAD^+)-glycohydrolase across the host cell membrane during infection; but interestingly this does not appear to be dependent on pore formation [10]. The average diameter of the SLO pore is 25-30 nm and is made up of 36-40 monomers [11–14]. Molecules of up to 150 kDa are able to diffuse though the pore in vitro [15,16].

SLO pores have been studied using electrochemistry in combination with surface plasmon resonance [17,18] and electron microscopy (EM) [11,12,14,19–21]. Kinetic data using radioactively labelled SLO on red blood cells suggests that binding is a first order process (with respect to surface site availability) and oligomerisation is a second order process limited by initial monomer–monomer dimerization [22]. Furthermore these data suggest that the SLO dimer inserts into the membrane and the pore then forms rapidly [20,22]. This is in contrast to the model described above which requires the formation of a complete uninserted pre-pore intermediate, which is thought to be more energetically favourable and represents the rate limiting step necessary for pore formation [7–9].

The mechanism of pore formation remains controversial because the pre-pore model cannot explain the incomplete pores (arcs) that are consistently observed by EM of membrane-bound SLO [11,12,14,19–21]. Instead these are dismissed as artefacts caused by the EM process [1]. Nevertheless SLO arcs are abundant and are thought to be functional [20]. If so, it is unclear whether pores simultaneously grow and insert, or incomplete pre-pores form and then insert into the membrane.

* Corresponding author at: Department of Biochemistry and Molecular Biology, Monash University, Clayton, Victoria 3800, Australia. Tel.: +61 3 9902 9365; fax: +61 3 9902 9500.
E-mail address: phil.bird@monash.edu (P.I. Bird).

http://dx.doi.org/10.1016/j.bbamem.2014.10.012
0005-2736/

Here we characterise SLO binding and pore formation by quartz crystal microbalance with dissipation monitoring (QCM-D). Unlike surface plasmon resonance, which provides little information about post binding events, QCM-D allows simultaneous measurement of mass accumulation and visco-elastic changes to the layer. QCM-D exploits the ability of AT-cut quartz to oscillate at a specific frequency when alternating current is applied. When a molecule adsorbs on the surface of the quartz-based sensor the frequency of oscillation decreases in proportion to the mass added. Simultaneously, the energy dissipated from the crystal can be measured, providing information about the viscoelasticity of the material on the surface. By covering the sensor with a lipid bilayer the rate of protein binding to mimetic mammalian membranes, and changes in membrane properties due to oligomerisation and pore formation, can be monitored in real time. We found that the binding/adsorption of SLO is concentration and cholesterol dependent. The initial binding proceeds at a single rate and fits the Langmuir isotherm model, indicating that there is no cooperation between monomers during this process. Through the use of various mutants we study the succeeding steps of pore formation, demonstrating that QCM-D can distinguish between binding and insertion. Using QCM-D with atomic force microscopy (AFM) we suggest that oligomerisation need not be complete for membrane insertion to occur.

2. Materials and methods

2.1. Materials

1, 2-dimyristoyl-sn-glycero-3-phosphocholine (DMPC) (cat. 850345P, Avanti polar lipids), cholesterol (Chol) (cat. C8667, Sigma-Aldrich), dithiothreitol (DTT) (cat. D9779, Sigma-Aldrich), L-α-phosphatidylcholine from egg yolk (eggPC) (cat. P3556, Sigma-Aldrich), 3-mercaptopropionic acid (MPA) (cat. M5801, Sigma-Aldrich), 30% hydrogen peroxide solution (cat. 108597, Merck Millipore), 28% ammonium hydroxide solution (cat. CAS 1336-21-6, Ajax Finechem), sodium dodecyl sulfate (cat. 0227, Amresco), Hepes (cat. 7365-45-9, Amresco), and NaCl (cat. 7647-14-5, Amresco).

2.2. Buffers

Hepes buffered saline (HBS) contains 20 mM Hepes, pH 7.5, and 150 mM NaCl; and low salt buffer (LS) contains 20 mM Hepes, pH 7.4, and 30 mM NaCl. All buffers were made up in double distilled water (MilliQ water) and then filtered through a 0.22 μm filter and degassed.

2.3. Proteins

The plasmid for expression of maltose binding protein (MBP)-SLO was a generous gift from Prof. S. Bhakdi. Recombinant SLO was made as described and used with MBP still fused to SLO [21]. Mutants were produced by Genscript and cloned in frame with MBP in pMALc2. Mutants were also produced as described [21]. Enhanced green fluorescent (eGFP) protein was made as described [23].

2.4. sRBC lysis assays

Sheep erythrocytes were washed in 0.9% saline solution to remove any contaminating haemoglobin in the buffer. The erythrocytes were then counted and resuspended at 2×10^8 cells/ml. SLO was serially diluted in HBS and 2×10^7 cells were added to each dilution in a final volume of 200 μl. This was then incubated at 37 °C or 22 °C for 20 min and supernatant collected and its absorbance measured at 405 nm to detect the release of haemoglobin.

2.5. Liposome preparation

Liposomes were prepared as described [24]. Briefly, DMPC, eggPC and cholesterol powder were dissolved in ethanol-free chloroform to make a 5 mM stock solution. Lipid mixtures were made up in a ratio of 40:60 (v/v) DMPC:Chol 50:50 (v/v) eggPC:Chol. Chloroform was evaporated under a gentle stream of nitrogen gas leaving a film of lipid on the wall of the test tube. Any remaining solvent was removed by placing the test tubes in a vacuum desiccator for 2 h and lipids were stored at −20 °C. Lipids were rehydrated in HBS to a final concentration of 0.5 mM at 37 °C for 1 h, vortexed for 2–5 min and sonicated in a water bath for 7 min 1–3 times at ~50 °C. Liposome suspensions were stored at 4 °C for up to 7 days.

2.6. Surface cleaning and modification

Gold coated sensors were cleaned by immersion in ammonium hydroxide:hydrogen peroxide:water (1:1:3 v/v) at 70 °C for 15–20 min as described [24]. The gold surface was modified by immersion in 1 mM MPA made in propan-2-ol for at least 1 h at room temperature. Silicon dioxide sensors were cleaned by immersion in 2% (w/v) SDS solution for 1 h at room temperature. The sensors were then rinsed with water and dried under a stream of nitrogen. Any remaining organic material was removed with UV-ozone treatment (3×10 min).

2.7. Quartz crystal microscopy with dissipation monitoring

QCM-D measurements were performed with the E4 system with flow cells (Q-Sense, Sweden) as described [24]. Briefly, changes to the resonance frequency (Δf) and energy dissipation (ΔD) were measured simultaneously. All plots presented represent the 7th harmonic unless stated. All experiments were conducted at 22 °C. Lipid was deposited until a change in frequency equals to 25–30 Hz was achieved as this corresponds to a fully covered sensor with a lipid bilayer [25]. When forming a bilayer on SiO_2 lipids are injected until a steady baseline was achieved. Washing with a low salt buffer (LS-HBS) generates osmotic stress to burst any intact liposomes. Once baseline is established in buffer the protein is added to the system by flowing it over the sensor at a rate of 50 μl/min. Once all the protein was used the flow was stopped and binding allowed to continue for at least 10 min before washing any unbound material off the surface with HBS at 300–500 μl/min. Unless stated, measurements were repeated at least 3 times, and representative traces are shown.

2.8. Atomic force microscopy

SiO_2 sensors modified with lipid and treated with SLO were taken directly from the QCM-D cells and immersed in HBS-LS. Sensors were then washed extensively by pipette with HBS-LS and placed in a glass petri-dish containing HBS-LS. Imaging was performed in contact mode using a JPK NanoWizard 3 Bioscience AFM, at a line scan rate of 4 Hz and a force set-point < 1 nN. This instrument is equipped with capacitive sensors to ensure accurate reporting of height, z, and x–y lateral distances. Cantilevers used were HYDRA6V-200W series from AppNano, with a nominal force constant and resonance frequency of 0.081 N/m and 17 kHz respectively.

2.9. Theoretical model

The change in mass (Δm) on the surface of the sensor can be calculated according to the Sauerbrey equation [26]:

$$\Delta m = -C(\Delta f/n)$$

where C is the mass sensitivity constant (in this case 17.7 ng/cm^2 for a sensor with a fundamental frequency of 5 MHz) and n is the harmonic

number (here we use the seventh (i.e. n = 7)). However the Sauerbrey equation assumes that the layer is rigid and even, and therefore it may not hold for hydrated layers providing an underestimate of the actual mass per unit area.

The kinetic form of the Langmuir adsorption model provides the simplest descriptor for the dynamics of adsorption at a solid–solution interface [27]:

$$\Gamma^{\max} = k^{\mathrm{ads}}(1-\theta)\left[M \cdot C_b + k^{\mathrm{des}}\theta/k^{\mathrm{ads}}(1-\theta) + M\right] - k^{\mathrm{des}}\theta$$

where $\Gamma^{\max}$ is the maximum adsorbed amount in mol/m^2 (solved using the Sauerbrey equation for a saturating concentration), M is a mass transport factor that represents how quickly molecules can get to the surface in ms^{-1}, k^{ads} is the rate of adsorption in ms^{-1}, k^{des} is the rate of desorption in mol/m^2/s^1 and C_b is the bulk concentration in mol/m^3. The fractional surface coverage, θ is calculated by dividing the adsorbed amount at a given time, $\Gamma(t)$ by the maximum adsorbed amount ($\Gamma^{\max}$). At low surface coverage, the adsorption process is assumed to be broadly controlled by diffusion of molecules to the surface, and so the initial slope of θ vs t, i.e. $d\theta/dt$ is used to calibrate M [28].

3. Results

3.1. SLO monomer binding to lipids is non-cooperative

We prepared recombinant SLO with maltose binding protein (MBP) fused to the N-terminus as previously described [21]. The N-terminal MBP was not removed as it has been shown previously to have no impact on pore formation [21]. We confirmed the biological activity of this SLO fusion protein via erythrocyte lysis at both 37 °C and 22 °C (Fig. 1A(i)). The recombinant protein is approximately 100 kDa and pure (Fig. 1A(ii)). We used QCM-D to study SLO binding and activity on DMPC:Chol membranes at 22 °C, using gold sensors modified with MPA (Au-MPA) to support the lipid bilayer. Changes in frequency and dissipation were monitored in real time as various concentrations of SLO flowed over the lipid-covered sensors. After the flow was stopped the sensor was monitored for any further changes for approximately 10–20 min, then washed with buffer to remove any unbound material (Fig. 1B). A decrease in frequency indicates protein binding to the lipid, and according to the Sauerbrey equation [26], mass accumulation is proportional to the change in frequency (Δf) (in this system the measured mass refers to hydrated mass). Changes in dissipation (ΔD) indicate alterations to the viscoelastic properties of the lipid–protein layer, where an increase in dissipation means the layer is becoming more energy-dissipating (fluid) and a decrease in dissipation means the layer is becoming less energy-dissipating (more rigid). These data can also be plotted as Δf vs. ΔD [29], which provides a 'signature trace' for SLO interactions on the sensor (Fig. 1C).

We observed concentration-dependent binding of SLO to the lipid layer, indicated by the decrease in frequency, with Δf following the same trend in increasing SLO concentrations and reaching saturation with 100 and 200 nM SLO (Fig. 1B). No change in frequency was observed during the final wash, indicating that SLO does not dissociate from the membrane (Fig. 1B). From these data the maximal mass of SLO bound to the lipid was calculated using the Sauerbrey equation. This yielded a maximal mass of 252.9 ng/cm^2 SLO bound to the lipid. However it is important to note that the Sauerbrey equation assumes that the layer is rigid and uniform and therefore may underestimate the actual mass per unit area.

As molecules of SLO bind and interact with the lipid layer ΔD increases, suggesting that the layer becomes more energy dissipating upon addition of SLO (Fig. 1B). The changes in dissipation are consistent with a more viscoelastic composition following binding of SLO. The most likely explanation is that bound SLO absorbs energy and dissipates it into the surrounding buffer. From the Δf vs. ΔD plot it is evident that as SLO binds to the membrane the frequency decreases and dissipation increases, and the shape of these traces remains very similar over various SLO concentrations (Fig. 1C).

We also analysed the first derivative of the frequency and dissipation functions for the concentrations of SLO plotted in Fig. 1B. This highlights subtle changes in the gradient of the frequency and dissipation functions, which may reflect binding to the membrane, conformational changes to the protein on the membrane, or other effects such as membrane changes including densification or solvation. The first derivatives of the frequency data ($\Delta f'$) indicate that two events (seen as minima) occur as SLO interacts with membrane. The first of these appears to be essentially concentration-independent, whereas the second appears to be strongly concentration-dependent (Fig. 1D). Similarly the first derivative of ΔD ($\Delta D'$) also shows two events (maxima) which appear to mirror $\Delta f'$ and indicates the viscoelasticity of the composite layer is changing due to SLO (Fig. 1D).

An interpretation of these two events consistent with available literature is that the first event corresponds to initial protein binding, and the second to lateral diffusion and oligomerisation. The latter process would free surface sites for further binding, thus explaining the large shifts in both frequency and dissipation.

To assess the overall rate of SLO binding we used the Δf data from the 200 nM SLO experiment and plotted this against the Langmuir isotherm adsorption model. 200 nM SLO was used for this analysis because all available binding sites are saturated (Fig. 1B). The data overlay with the Langmuir adsorption isotherm curve, reflecting a single rate of binding, with no evidence for cooperative binding as the concentration of monomers on the surface increases (Fig. 1E). This is consistent with previous data where monomers first bind to the membrane and then laterally diffuse to oligomerise and form pores [5,6,17,22,30]. It is also consistent with the first derivative analysis (Fig. 1D) as this highlights subtle deviations in the protein–membrane interaction that can be attributed to changes in the protein conformation once it is already bound to the lipid bilayer.

The QCM-D system also allows changes on the sensor to be monitored over various harmonics. The closer to the sensor's surface, the higher the harmonic number because at higher harmonics the magnitude of oscillation decreases and therefore only probes material close to the sensor surface. Variation in Δf and ΔD in the different harmonics has been observed with small, lipid-penetrating peptides [31]. We monitored the 3rd, 5th, 7th and 9th harmonics in this study. As illustrated by traces obtained for 100 nM SLO, overall there was little difference between the harmonics in either dissipation or frequency (Fig. 1F). There was however a small but reproducible spread in these harmonics for the frequency which may reflect more mass on the surface of the lipid (3rd harmonic), compared to very close to the sensor's surface (9th harmonic). The signature Δf vs. ΔD trace showed the same trend over the 4 harmonics (Fig. 1G). We conclude that the limited variation in the harmonic read-out, compared to other studies using peptides, is probably due to the much larger size of SLO. Therefore we only display the 7th harmonic data for subsequent experiments, as it is less prone to interference/noise (which can be seen as the magnitude of oscillation increases). In subsequent experiments conducted with 100 nM SLO, curves were consistent and reproducible, and any slight variation in Δf or ΔD is assumed to be due to variation in the lipid layer formed on the day (Fig. S1A). Importantly, Δf vs. ΔD plots overlay and are reproducible across multiple measurements (Fig. S1B).

To rule out effects of non-specific binding of SLO or trace proteins to the DMPC:Chol lipid layer, or to any exposed MPA, we compared SLO binding to eGFP binding. eGFP was chosen because it is not membrane active and has a neutral pI [23]. When eGFP was introduced into the QCM-D cell a small and transient decrease in Δf (−15 Hz) was observed, which quickly returned to zero (Fig. 1H). There was no change in the dissipation, and no further changes during the incubation or washing periods. This trace represents a negative control showing that protein does not non-specifically adsorb to the lipid layer,

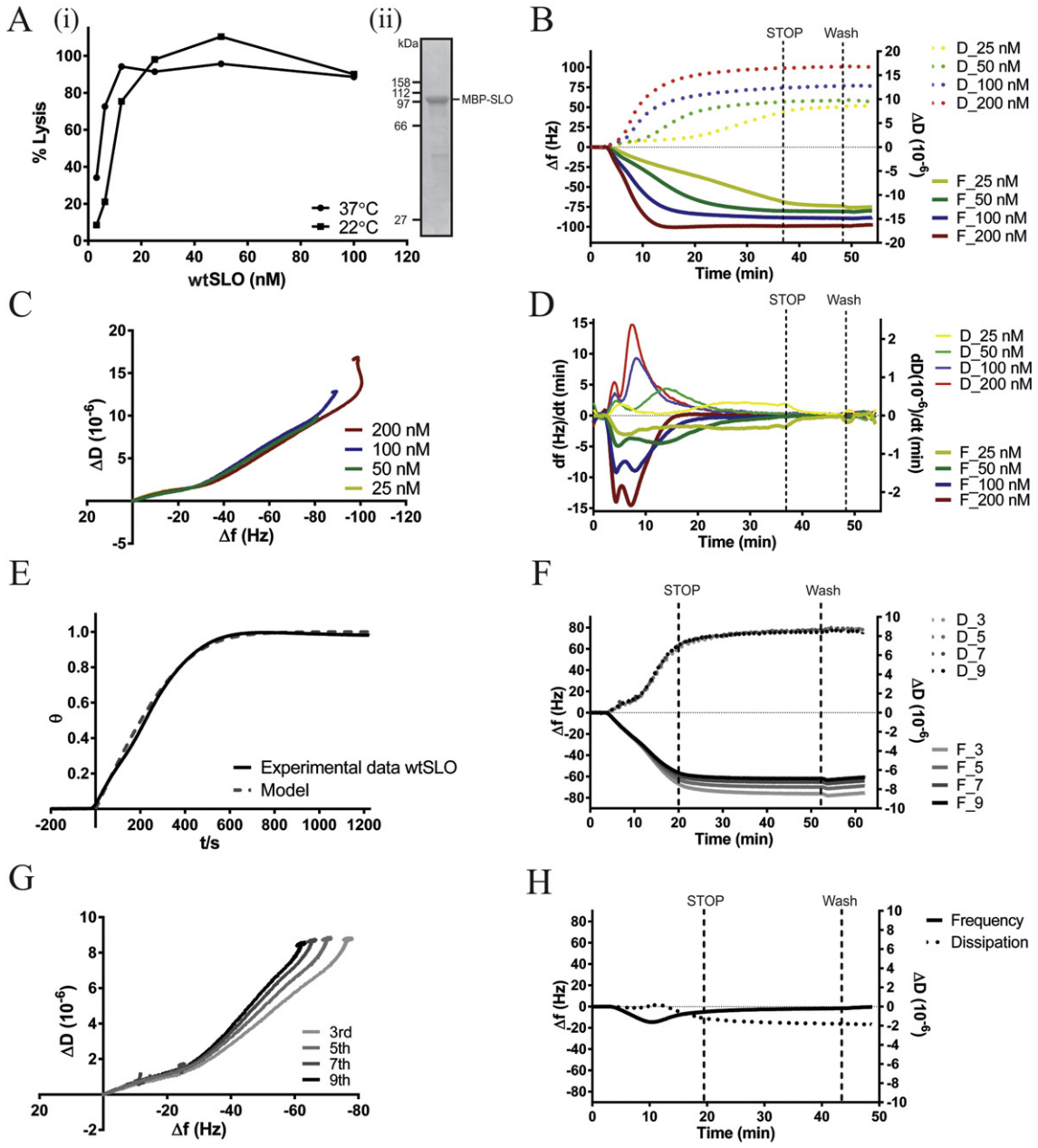

Fig. 1. Binding and activity of wtSLO on DMPC:Chol membranes assessed by QCM-D. A)(i) Increasing concentrations of recombinant wtSLO was tested on sRBC for lytic activity at 22 °C (squares) and 37 °C (circles). (ii) Recombinant wtSLO (2 μg) resolved by SDS-PAGE. B) Au–MPA sensors with a DMPC:Chol (40:60) bilayer with increasing concentrations of wtSLO (25–200 nM) were introduced at 50 μl/min over a total volume of 2 ml. Flow was stopped for 10 min (STOP) to allow the protein to incubate, the cell was then washed with HBS at 300 μl/min (Wash). The change in frequency in Hertz (Δf) is plotted on the left axis as solid lines and the change in dissipation (ΔD) is plotted on the right axis as broken lines, concentrations are indicated. C) WtSLO Δf–ΔD signature traces. Data from panel (B) is replotted as Δf on the x-axis verses ΔD on the y-axis. D) The first derivative of the frequency and dissipation as plotted in (B). The first derivative of the frequency (df (Hz)/dt (min)) is plotted on the left hand side with the functions in darker colours and the first derivative of the dissipation (dD (10^{-6})/dt (min)) is plotted in the right in lighter colours. E) The wtSLO binding rate overlays the Langmuir isotherm model of absorption. Data from panel (B) for 200 nM wtSLO is plotted as theta (θ) against the Langmuir isotherm absorption model over time. F) The effect of 100 nM wtSLO on the 3rd, 5th, 7th and 9th harmonics, Δf is plotted on the left axis and ΔD is plotted on the right. The harmonic extending furthest from the surface of the sensor (3rd) is plotted as the lightest grey line, increasing in darkness to the (9th) harmonic which is closest to the sensor surface. G) Δf–ΔD signature trace for 100 nM wtSLO over the various harmonics, the 3rd is plotted as light grey increasing in darkness to the 9th. H) QCM-D characterisation of 100 nM eGFP on DMPC:Chol. Data plotted as per panel (B).

and demonstrates that the binding (Δf) and rearrangement (ΔD) seen with SLO reflect its authentic biological function and not non-specific protein–lipid or protein–MPA interactions.

3.2. Cholesterol is required for maximal SLO binding

A defining characteristic of the CDCs is cholesterol binding. To determine if this is recapitulated in the QCM-D system, we prepared lipids with or without cholesterol and analysed SLO binding. A concentration of 60 %mol cholesterol was chosen because it has been reported that the CDCs do not bind membranes containing less than 45 %mol cholesterol and show maximal binding at 55 %mol [32,33]. To assess the cholesterol dependence of SLO we used 100 nM SLO on DMPC alone, or on DMPC containing 20 %mol, 40 %mol or 60 %mol cholesterol. On DMPC alone there was limited binding ($\Delta f = -35$ Hz) (Fig. 2A). Of the cholesterol concentrations tested, a major increase in mass accumulation ($\Delta f = -75$ Hz) was observed only at 60 %mol cholesterol, in agreement with previous data [32,33]. This was also reflected in the Δf

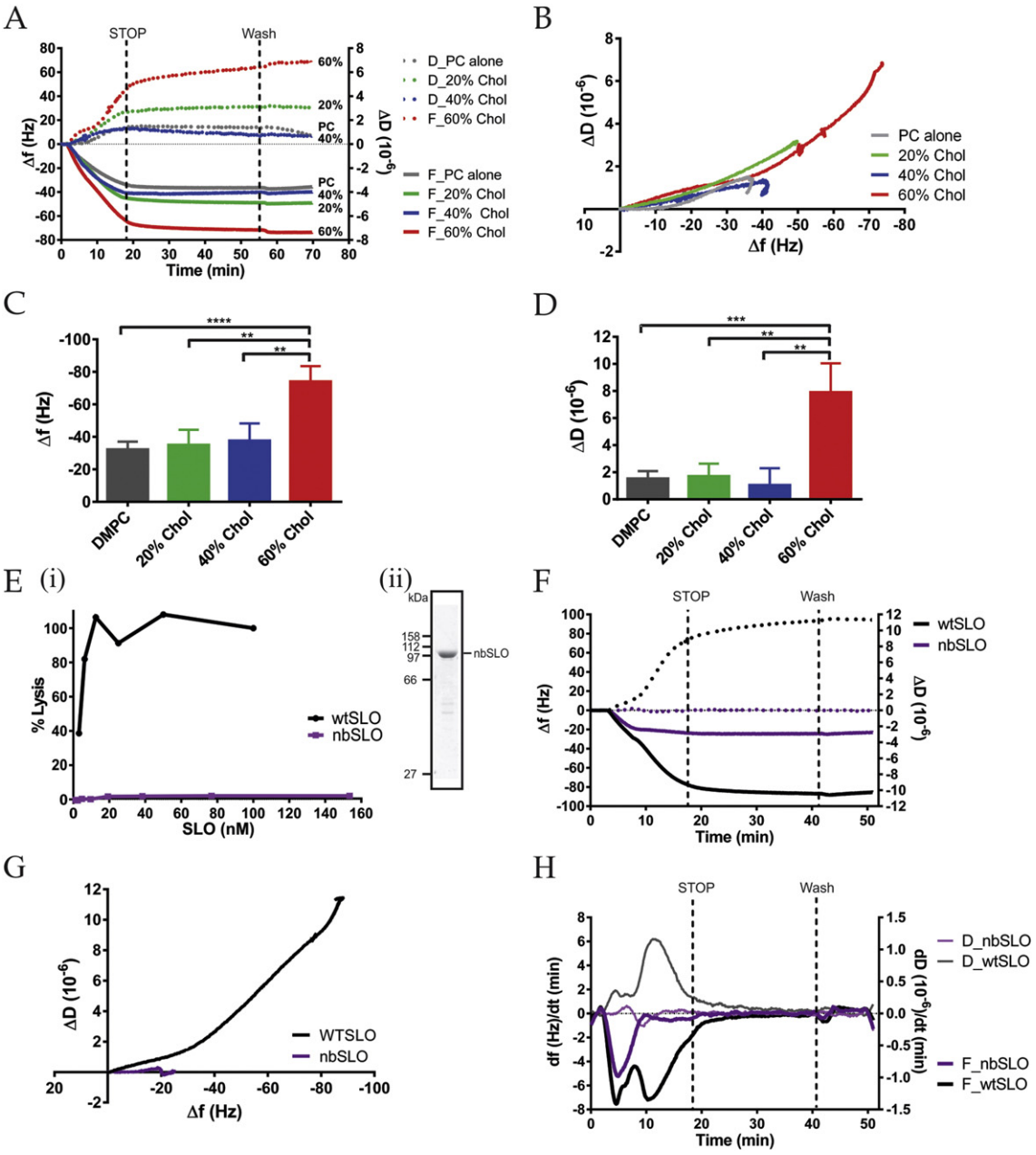

Fig. 2. WtSLO binding and activity on lipid membranes is dependent on cholesterol. A) QCM-D trace of 100 nM wtSLO on increasing concentrations of cholesterol (percentages indicated) in DMPC membranes, on Au–MPA. Δ*f* is plotted as solid lines and Δ*D* is plotted a dotted lines. B) Δ*f*–Δ*D* trace for 100 nM wtSLO on PC alone (grey), PC with 20% cholesterol (green), PC with 40% cholesterol (blue) and PC with 60% cholesterol (red). Data from panel A. C) Bar graph of the maximal Δ*f* after binding for DMPC (n = 4), DMPC:Chol 20% (n = 3), DMPC:Chol 40% (n = 3) and DMPC:Chol 60% (n = 5). Error bars represent the standard deviation from the mean. *p < 0.05, **p < 0.01, ***p < 0.001 and ****p < 0.0001 in a two tailed Student's *t* test. D) Bar graph of the maximal Δ*f* after binding for DMPC (n = 4), DMPC:Chol 20% (n = 3), DMPC:Chol 40% (n = 3) and DMPC:Chol 60% (n = 5). Statistical analysis as in B. E)(i) sRBC lysis assay comparing wtSLO and no binding mutant SLO. Increasing concentrations of wtSLO (black) and nbSLO (purple) are plotted as % lysis where 100% is the lysis seen in detergent treated sRBCs. (ii) Recombinant nbSLO (2 μg) resolved by SDS-PAGE. F) QCM-D trace of 100 nM wtSLO (black) and nbSLO (purple) on Au–MPA sensors with a DMCP:Chol bilayer. Data plotted as per panel (A). G) Δ*f*–Δ*D* trace for 100 nM wtSLO (black) and nbSLO (purple). Data from panel F. H) The first derivative of nbSLO (purple) and wtSLO (black) for the frequency and dissipation functions plotted in D. *df* (Hz)/*d*t (min) is plotted on the left hand side with the function in darker colours and *dD* (10^{-6})/*d*t (min) plotted on the right in lighter colours.

vs. Δ*D* trace (Fig. 2B). When the maximal values for Δ*f* and Δ*D* are plotted from several individual experiments it is clear that there is no difference between the concentrations of cholesterol until 60 %mol (Fig. 2C and D). The average amount of SLO binding in the absence of cholesterol is approximately 40% of that seen with 60% mol cholesterol. This indicates that while high concentrations of cholesterol significantly increase SLO binding to the membrane, cholesterol is not essential for SLO binding to DMPC.

We also made a 'no binding' mutant SLO (nbSLO) based on mutations made in PFO to render it incapable of binding cholesterol [2]. We mutated both T564 and L565 to glycine and the resulting purified mutant displayed no haemolytic activity (Fig. 2E). However when assessed by QCM-D on Au–MPA with DMPC:Chol we detected significant binding (Fig. 2F), at a level similar to wtSLO on DMPC alone (shown in Fig. 2A). There was no change in the dissipation, unlike wtSLO on DMPC alone where an increase in dissipation is observed. The differences between wtSLO and nbSLO are highlighted in the Δ*f* vs. Δ*D* trace (Fig. 2G).

In the first derivative analysis of the frequency data (Fig. 2H) the limited binding seen in Fig. 2F corresponds to the first event seen for wtSLO.

It would appear that Δ*f*′ does not reach the same magnitude, and the second event is completely absent. No clear events occurred in the dissipation with this mutant (Fig. 2F and H). This indicates that the first event is monomer binding (whether through cholesterol or another lipid element) and the second reflects a subsequent step in wtSLO pore assembly.

3.3. QCM-D traces reflect SLO rearrangement into pores

We next examined whether rearrangement and assembly of SLO into pores was occurring on the sensor and contributing to the changes in frequency and dissipation observed in QCM-D. Formation of pores should alter the conductance of the sensor as measured by cyclic

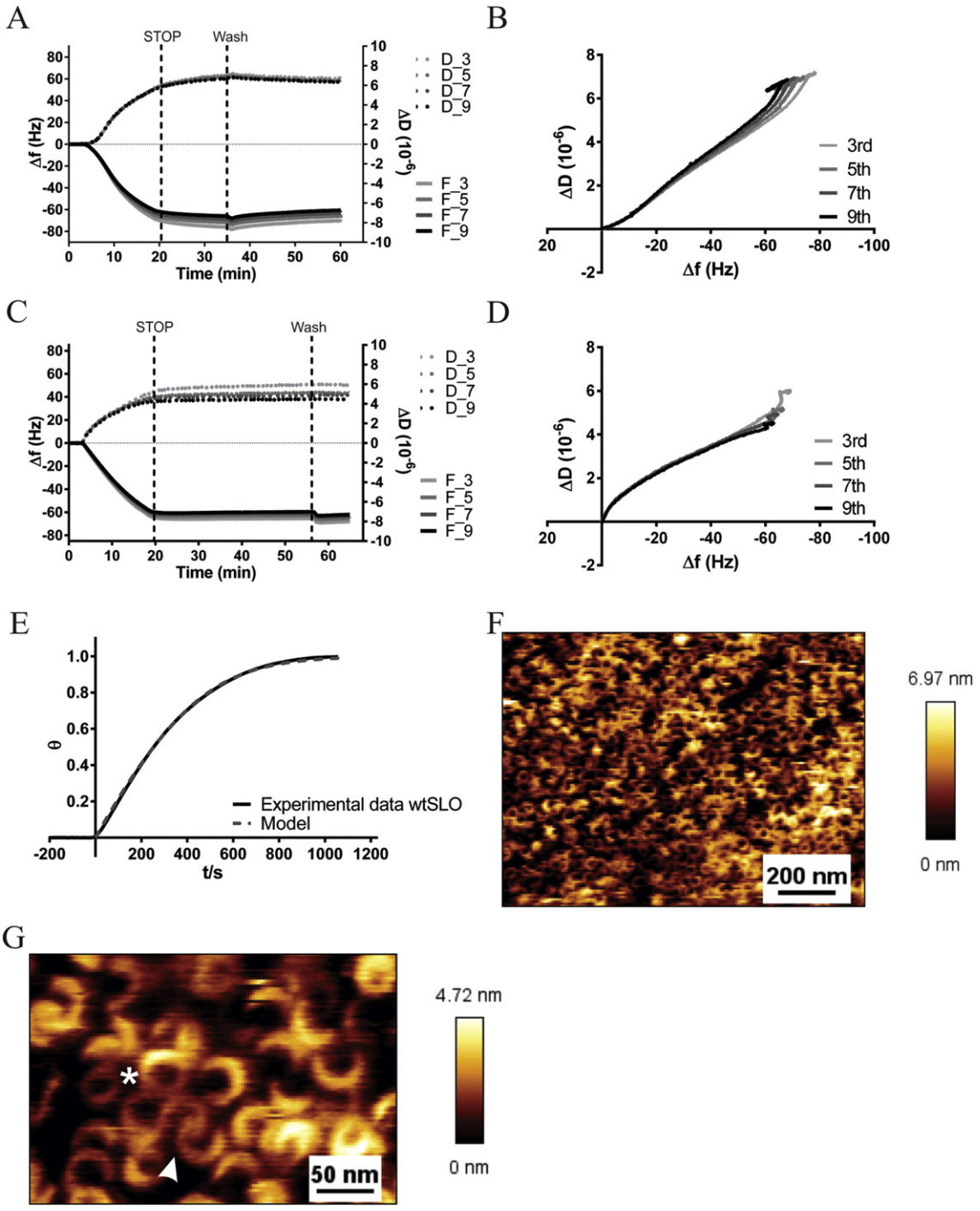

Fig. 3. wtSLO pore formation in QCM-D. A) Trace for 100 nM wtSLO on Au–MPA with an eggPC:Chol (50:50) bilayer, Δ*f* is plotted as solid lines and Δ*D* as dotted lines (n = 2). Harmonics are graded darkest for closest to the sensors surface to lightest for furthest from the sensors surface. B) Δ*f*–Δ*D* trace for 100 nM wtSLO on Au–MPA with an eggPC:Chol (50:50) bilayer. Data from panel A.C) 100 nM wtSLO on SiO_2 with an eggPC:Chol (50:50) bilayer, Δ*f* is plotted as solid line and Δ*D* plotted as dotted lines. Different harmonics are represented as per panel (A). D) Δ*f*–Δ*D* trace for 100 nM wtSLO on SiO_2 with an eggPC:Chol (50:50) bilayer. Data from panel C. E) WtSLO binding to eggPC:Chol overlays the Langmuir isotherm model of absorption. Experimental data for 300 nM wtSLO is plotted as theta (θ) against the Langmuir isotherm absorption model over time. F) AFM image of 100 nM wtSLO on SiO_2 eggPC:Chol (50:50) taken from the QCM-D flow cell. G) AFM image, conditions as in (F), smaller scan from a different experiment. Interlocking incomplete pores are indicated by the white arrow head, full pores are located either side of the asterisk.

voltammetry [34], and pores should be evident via atomic force microscopy (AFM) [7]. However, we found the Au–MPA sensors unsuitable for conductance measurements, and they are also too rough for AFM. To circumvent these problems we conducted QCM-D experiments on SiO_2 sensors, which are atomically flat and suitable for AFM. We used L-α-PC from chicken egg yolk (eggPC) as the source of PC because DMPC deposited onto SiO_2 sensors do not bind SLO, indicating cholesterol is either not incorporated into the lipid bilayer or it is inaccessible (data not shown). To ensure that the interaction of SLO with eggPC head groups was no different to its interaction with DMPC head groups we tested SLO with eggPC:Chol on Au–MPA sensors. The QCM-D traces for 100 nM SLO on eggPC:Chol (Fig. 3A and B) and DMPC:Chol (Fig. 1F and G) on Au–MPA sensors were comparable. The QCM-D trace for SLO on eggPC:Chol-coated SiO_2 sensors showed slightly different frequency and dissipation traces compared to eggPC:Chol coated Au–MPA sensors (Fig. 3C and D). This is more obvious in the small spread in the different harmonics for the dissipation on SiO_2 (Fig. 3C). The Δf–ΔD trace under these conditions was also slightly different, indicated by the shape of the trace (Fig. 3D). However the overall shape of the Δf–ΔD trace was the same (Fig. 3D). We speculate that these small differences reflect higher sensitivity of the SiO_2 sensors, or differences in membrane structure/fluidity on the two substrates. Nevertheless the kinetics of SLO binding to the eggPC:Chol membrane were essentially the same as on Au–MPA with DMPC:Chol, and also fit the Langmuir adsorption isotherm (Fig. 3E). Hence we continued with eggPC:Chol on SiO_2 sensors for the AFM studies.

AFM images of SiO_2 sensors taken from the QCM-D instrument after SLO binding revealed canonical pore structures, similar to those reported for PFO [7]. Importantly, we observed a mixture of full ring structures and partial ring structures (also termed arcs [11,20]) that often interlocked (Fig. 3F and G). The full ring structures were approximately 30 nm in diameter, consistent with previous reports of the size of the SLO pore [11–14], however we were unable to measure the height of these structures because they covered the lipid completely, preventing establishment of an accurate baseline. Nevertheless, these images clearly demonstrate that the changes in frequency and dissipation measured by QCM-D as SLO interacts with lipid capture the entire process of binding, oligomerisation and pore formation.

3.4. Monomer-locked SLO changes the QCM-D signature

To probe the self-assembly process from monomers to pores we made a 'disulfide-locked monomer' mutant SLO (dsmSLO) containing T393C and V408C substitutions, also based on mutations made previously to PFO [30]. These mutations create an internal disulfide bridge inhibiting monomer–monomer interactions. This disulfide bridge can be reduced allowing monomer–monomer interactions and pore formation to proceed normally.

Although not completely pure, recombinant dsmSLO was validated with sRBC lysis assays, and these showed that it was not lytic unless treated with DTT to reduce the disulfide bond (Fig. 4A). Once reduced, dsmSLO was as active as wtSLO on red blood cells (Fig. 4A). To assess the binding and activity of dsmSLO by QCM-D, we compared untreated and DTT pre-treated wtSLO and dsmSLO on DMPC:Chol. DTT did not affect wtSLO (Fig. 4B), and as expected reduced dsmSLO was indistinguishable from wtSLO in both Δf and ΔD (Fig. 4C). The non-reduced dsmSLO also looked very similar to wtSLO in Δf, however there was a small but reproducible difference in ΔD in the form of a shift to the left and a smaller total ΔD (Fig. 4C). This is also evident when the data is plotted as Δf vs. ΔD: the signatures of wtSLO (+/− DTT) and reduced dsmSLO overlay, whereas non-reduced dsmSLO does not overlay the wtSLO trace (Fig. 4D).

It is expected that non-reduced, non-oligomerising dsmSLO would be more hydrated than the reduced, oligomerising form because water molecules would be lost during monomer–monomer binding and oligomerisation. There is a small difference in the final Δf value when the flow is stopped (and during binding) between the reduced and non-reduced forms of dsmSLO. The reduced dsmSLO has a larger Δf value indicating that less mass has been acquired on the sensor. This was assessed over several experiments, and although the mean Δf of dsmSLO appears lower (has a more negative Δf so more mass) compared to the reduced dsmSLO, this is not statistically significant (Fig. S2A). ΔD is slightly lower for dsmSLO compared to reduced dsmSLO, again this is not significant (Fig. S2B).

Furthermore when the first derivative of Δf is plotted it is clear that these proteins differ. The first event for the dsmSLO overlays with the wtSLO data but the second event is not apparent (Fig. 4E). The second event however is evident in the reduced dsmSLO (Fig. 4E). The final minimum of the reduced dsmSLO is not the same as wtSLO; we suggest that this may be due to incomplete reduction of the mutant disulfide bond. Interestingly there are still two clear events in the first derivative of ΔD for dsmSLO, however in contrast to wtSLO and reduced dsmSLO the second event appears to occur earlier in the adsorption cycle (Fig. 4E).

The differences between non-reduced and reduced dsmSLO were more pronounced on SiO_2 eggPC:Chol. Less of the non-reduced dsmSLO bound to the lipid initially, and it dissociated from the lipid during the wash step. By contrast, reduced dsmSLO remained bound to the surface (Fig. 4F). These data also show a shifted signature trace when plotted as Δf vs. ΔD (Fig. 4G). Together these results indicate that for stable binding to the bilayer, SLO must actively rearrange.

3.5. Pre-pore locked SLO displays a similar profile to monomer-locked SLO

To distinguish oligomerisation from pore formation we made the pre-pore locked mutant SLO (ppSLO) described previously [10]. This mutant is reported to oligomerise into a ring structure that cannot puncture the membrane. When assessed by sRBC lysis assays the lytic ability of the mutant was reduced but not completely abolished. Nevertheless, there was a 17-fold increase in the concentration of ppSLO required to lyse 50% of red blood cells compared to wtSLO (Fig. 5A). When compared to wtSLO, by QCM-D, ppSLO binds faster than wtSLO and reaches a plateau earlier (Fig. 5B). There was also a difference in the dissipation between wt and ppSLO (Fig. 5B), similar to that seen for dsmSLO (Fig. 4C), and the signature of the Δf vs. ΔD plot (Fig. 5C) changed in a similar way to dsmSLO (Fig. 4D). When the first derivatives of these functions were assessed, it was evident that the ppSLO displays two events for both the $\Delta f'$ and $\Delta D'$, similar to wtSLO. The second minimum however, occurred earlier in both the $\Delta f'$ and $\Delta D'$ (Fig. 5D). This change in dissipation is again very similar to that of the dsmSLO mutant where the second event (maximum) occurs earlier than that for wtSLO. Monomer binding remains a single-order process as determined by fitting into the Langmuir isotherm equation (Fig. 5E).

When using eggPC:Chol on SiO_2 there was also more efficient ppSLO binding to the lipid as well as differences in the dissipation, again shifted towards the left (Fig. 5F). However the most interesting feature of this trace was that ppSLO dissociated from the lipid easily and completely (Fig. 5F), similar to dsmSLO (Fig. 4F). This again suggests that in order to stably bind to the lipid surface, SLO must be conformationally competent to self-assemble into membrane-penetrating structures. When these data were plotted as Δf vs. ΔD it was again apparent that the ppSLO signature differs from wtSLO, in a similar vein to the difference seen with dsmSLO (Fig. 5G).

4. Discussion

Here we have probed the mechanism of SLO pore formation on lipid bilayers using QCM-D. We found that SLO adsorption and binding behaviour are concentration and cholesterol dependent, and that the kinetics are consistent with the Langmuir isotherm model. Through changes to the QCM-D signature exhibited by SLO mutants we can

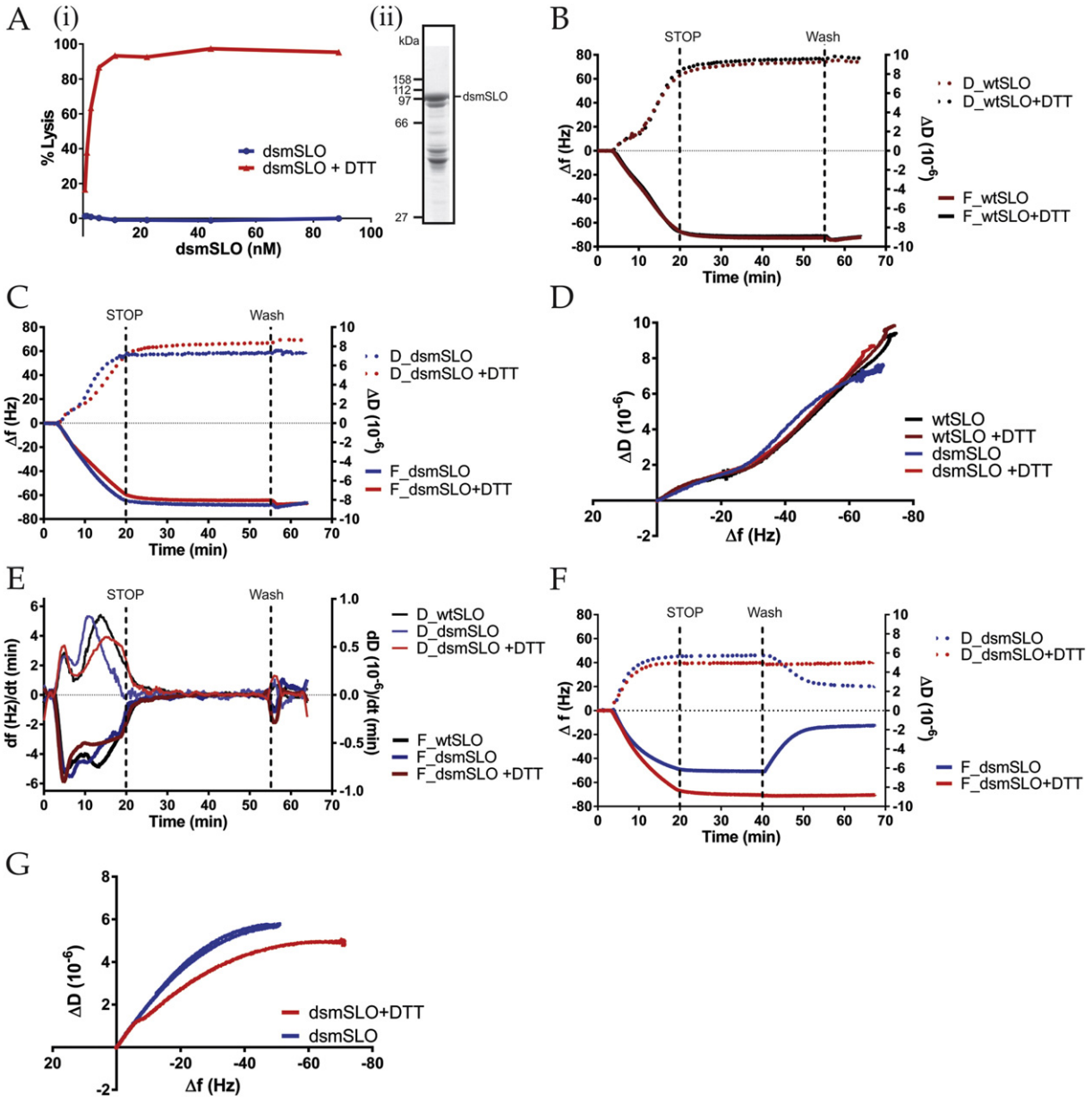

Fig. 4. Effect of monomer locked SLO binding assessed by QCM-D. A)(i) sRBC lysis assay of increasing concentrations of reduced (red) and non-reduced (blue) disulfide locked monomer mutant SLO (dsmSLO). (ii) Purified dsmSLO (2 μg) resolved by SDS-PAGE. B) QCM-D trace on Au–MPA with a DMPC:Chol bilayer of 100 nM wtSLO pre-treated with DTT (dark red) and 100 nM untreated wtSLO (black). Δ*f* (solid lines) is plotted on the left axis and Δ*D* (broken lines) is plotted on the right. C) QCM-D trace on Au–MPA with a DMPC:Chol bilayer of 100 nM dsmSLO pre-treated with DTT (red) and 100 nM untreated dsmSLO (blue), plotted as per panel (B). D) Δ*f*–Δ*D* signature trace of wtSLO (black), reduced wtSLO (dark red), dsmSLO (blue) and reduced dsmSLO (red). Data from panels (B) and (C) are replotted as Δ*f* on the x-axis verses Δ*D* on the y-axis. E) The first derivative of the dsmSLO (blue), reduced dsmSLO (red) and wtSLO (black) functions for frequency and dissipation plotted in (B and C). *df* (Hz)/*dt* (min) is plotted on the left hand side with the function in darker colours and *dD* (10^{-6})/*dt* (min) plotted on the right in lighter colours. F) QCM-D trace of 100 nM dsmSLO reduced (red) and non-reduced (blue) on SiO_2 sensors with an eggPC:Chol bilayer. Δ*f* and Δ*D* plotted as per panel (B) (n = 2). G) Δ*f*–Δ*D* signature trace for 100 nM reduced (red) and non-reduced (blue) dsmSLO on SiO_2 with an eggPC:Chol bilayer (n = 2), plotted as per panel (F).

distinguish between binding/rearrangement and insertion. This makes QCM-D an excellent tool to study the dynamics of pore formation.

4.1. SLO binding

Analysis of Δ*f* confirms that SLO binding to lipids proceeds in a concentration-dependent manner that is enhanced by cholesterol. Using these data we can investigate the kinetics of binding to the lipid layer because Δ*f* is proportional to the accumulation of mass according to the Sauerbrey equation [26]. We found that when the decay of available binding sites (probably cholesterol) is accounted for, there is only one rate of binding, consistent with the Langmuir isotherm adsorption model. Wilkop and colleagues have previously hypothesized that SLO binding would fit this model [17], and here, using QCM-D, we have demonstrated that this is indeed realized. Other kinetic analyses by Palmer and colleagues also demonstrate that binding to red blood cells is a single order process and is non-cooperative [22]. Thus we add to the body of evidence that demonstrates that SLO monomers first bind to the membrane and then undergo a structural change that allows oligomerisation and perforation to proceed [5,6,17,22,35].

In addition to analyzing the overall rate of binding we also analysed the first derivative of the frequency and dissipation. We find that there are changes to the gradients of these functions that are not large enough to change the overall binding profile significantly. These probably reflect

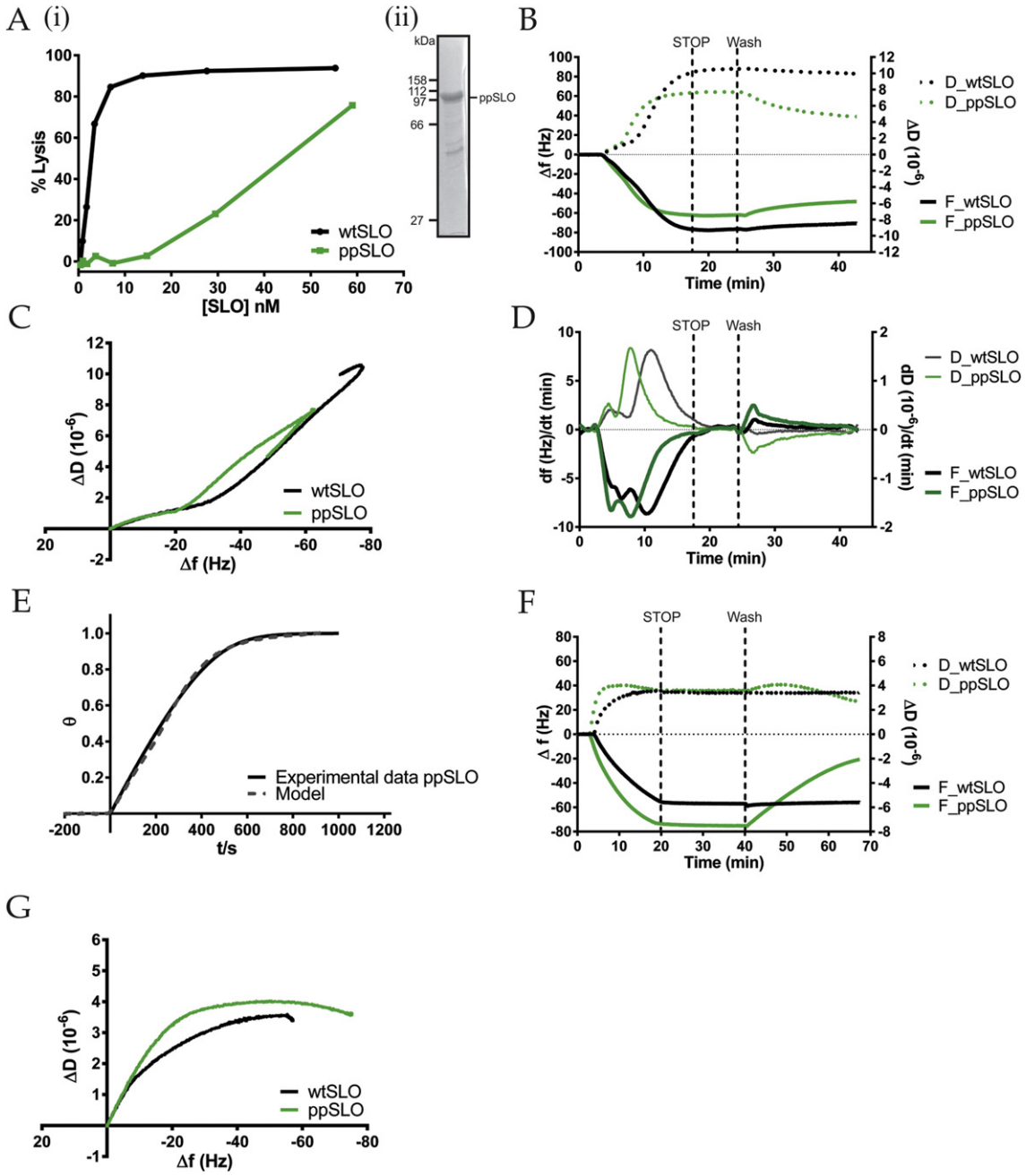

Fig. 5. Pre-pore locking SLO changes the QCM-D signature similarly to monomer locked SLO. A)(i) sRBC lysis assay with increasing concentrations of wtSLO (black) and ppSLO (green). (ii) ppSLO (2 μg) resolved by SDS-PAGE. B) QCM-D trace on Au–MPA with a DMPC:Chol bilayer of 100 nM each of ppSLO (green) and wtSLO (black). Δ*f* (solid lines) is plotted on the left axis and Δ*D* (broken lines) is plotted on the right. C) Δ*f*–Δ*D* signature trace of wtSLO (black) and ppSLO (green). Data from panel (B) replotted as Δ*f* on the x-axis verses Δ*D* on the y-axis. D) The first derivative of the ppSLO (green) and wtSLO (black) functions for frequency and dissipation plotted in (B and C). *df* (Hz)/*dt* (min) is plotted on the left hand side with the function in darker colours and *dD* (10^{-6})/*dt* (min) plotted on the right in lighter colours. E) The ppSLO binding rate overlays the Langmuir isotherm model of absorption. Data from panel (B) for 100 nM ppSLO is plotted as theta (θ) against the Langmuir isotherm absorption model over time. F) QCM-D trace of 100 nM wtSLO (black) and ppSLO (green) on SiO_2 sensors with an eggPC:Chol bilayer (n = 2). Δ*f* and Δ*D* plotted as per panel (B). G) Δ*f*–Δ*D* signature trace plotted as per panel (C) for wtSLO (black) and ppSLO (green) on SiO_2 with an eggPC:Chol bilayer, data from panel (F).

more subtle changes due to coupling between events such as binding, loss of coupled water from the protein and conformational changes of the protein on the membrane surface in real time. For wtSLO, two events occurred during binding, the first of which was significantly less concentration dependent than the second. We hypothesize that the first minimum/maximum corresponds to the initial binding of monomers to the membrane, whereas the second minimum/maximum relates to the oligomerisation and insertion process. The reasons that lead to this hypothesis are discussed below.

The first derivative of the dsmSLO mutant trace fails to make a clear transition into the second minimum for Δ*f*′, which can be corrected by reducing dsmSLO, whereas the ppSLO mutant clearly shows this second minimum (event). Δ*D*′ does not exactly mirror Δ*f*′ as the dsmSLO mutant still displays two clear events however, analogous to the ppSLO mutant, the second maximum occurs much earlier than the wtSLO. This shift in Δ*D*′ is reversed when using reduced dsmSLO: here the second event occurs later and the timing is similar to wtSLO. We suggest that the first event represents binding to the membrane, and the second

event reports the diffusion and oligomerisation of monomers on the surface of the membrane. The ppSLO mutant displays this second event earlier than wtSLO. We propose that in the wtSLO and reduced dsmSLO mutant oligomerisation and insertion events occur contemporaneously. This influences the rate of monomer diffusion and interaction with oligomers, which is reflected in the timing of the second maximum. For the ppSLO one explanation for earlier oligomerisation may be that there are more incomplete oligomers on the surface of the chip. As these cannot insert they provide more sites for monomer–monomer interactions and hence drive oligomerisation faster. By contrast, wtSLO oligomers can probably insert into the membrane without completing a full ring structure, as indicated by the arcs seen by AFM. If inserted oligomers cannot accept more monomers, oligomerisation must slow as available monomer–monomer interaction sites decrease.

Another explanation for the differences between $\Delta f'$ is that there are 3 minima: one observed with dsmSLO representing binding, the second only seen with ppSLO representing oligomerisation and the third identified with wtSLO representing overlapping oligomerisation and insertion processes as described above. The second minimum is only seen with the ppSLO as in the wtSLO it merges and shifts into the third minimum (which represents insertion).

The first derivative is very useful for identifying small changes in the frequency and dissipation, which have allowed us to highlight differences between the mutants. The data fit with previous kinetic data for SLO self-assembly, where binding is one clear event with a single rate and oligomerisation/insertion is a second event with a separate rate which is limited by the formation of an intermediate [22].

4.2. Dissecting the rearrangement process

The current model for CDC pore formation invokes three main steps (Fig. 6): 1. Cholesterol-dependent binding of monomers to the membrane. 2. Monomer rearrangement/lateral diffusion on the membrane to bind other monomers or oligomers and form a pre-pore structure. Implicit in this step is that the tightness of the association of the growing (non-inserted pre-pore) with the membrane increases with the addition of each subunit. 3. Conformational change involving vertical collapse to form a transmembrane pore or arc.

Mutants that arrest at various points were used to provide further information about pore formation. The first step in this process is binding to the membrane via cholesterol, therefore we studied a mutant (nbSLO) unable to bind cholesterol [2]. We observed less binding to the membrane, and pore formation was inhibited at the first step (Fig. 6 step 1). Interestingly, SLO on DMPC alone and nbSLO on DMPC:Chol behave slightly differently: both show less binding compared to wtSLO (~43% and 33% respectively). However unlike wtSLO the nbSLO mutant does not show an increase in the dissipation. This may indicate that the orientation of the protein on the surface or the interaction with the lipid layer is different when cholesterol-binding residues are mutated. Perhaps these sites also interact with DMPC in some circumstances.

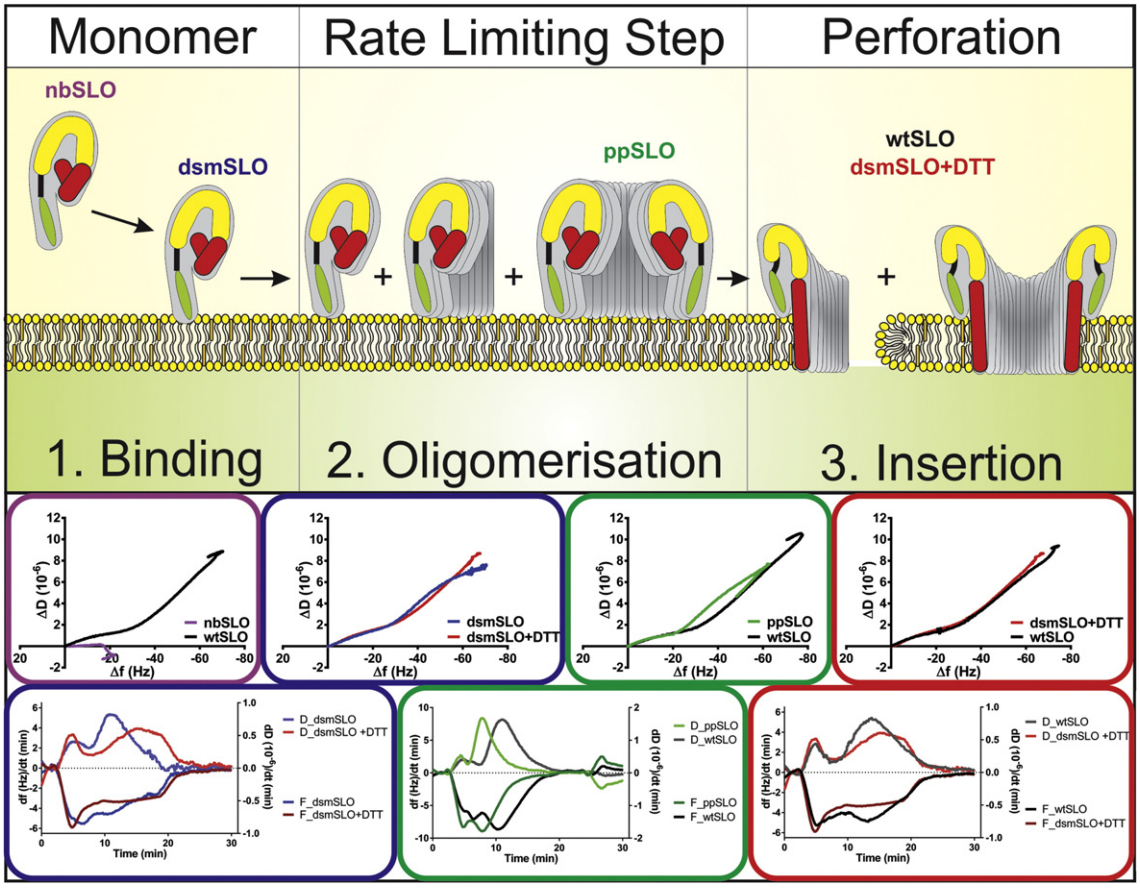

Fig. 6. Model for streptolysin O pore formation. Soluble monomers bind to the membrane through cholesterol specific residues in domain 4 (green) (1. Binding). Once bound the monomer diffuses laterally to bind other membrane bound monomers to form a growing circular complex (2. Oligomerisation). At some point during oligomerisation after a subunit threshold is reached (rate limiting step), whether it be dimer, half a ring or when ring formation is complete, two bundles of helices (red) from each monomer unravel to form beta hairpins that puncture the membrane and form the walls of the pore. This is accompanied by a vertical collapse due to changes in the MACPF domain (yellow). The existence of arcs suggests that oligomerisation cannot continue once membrane insertion has occurred (3. Insertion). Under each step depicted in this pathway a corresponding QCMD Δf–ΔD trace is shown as well as the first derivative (both frequency and dissipation) of dsmSLO, ppSLO and wtSLO to illustrate how these steps can be distinguished through the use of mutants which halt the process at various points.

This interaction with DMPC is SLO specific as eGFP does not bind any membrane on Au–MPA and is washed off easily, arguing against non-specific protein-MPA interactions. Clearly SLO is able to bind to membrane in the absence of cholesterol, whether this is important for SLO function remains unclear.

The next step in the process is association and rearrangement of bound monomers via lateral diffusion (Fig. 6 step 2), which we studied by inhibiting monomer–monomer interactions using a disulfide-locked monomer SLO mutant [30]. We showed that the initial binding (Δf) is generally unaffected but the $\Delta f'$ trace indicated that there is a lack of a clear second minimum, which is therefore likely to represent oligomerisation. Furthermore the effects on lipid viscoelasticity, ΔD, differ from wtSLO in that the change is faster and of lower total magnitude (this was more obvious in $\Delta D'$ and signature trace (Δf vs. ΔD)). These differences were reversed when the disulfide bridge ('lock') was reduced, allowing the process of pore formation to proceed from step 1 through to completion (Fig. 6). To separate the effects of oligomerisation (step 2) and insertion (step 3) we used a pre-pore locked mutant which is able to oligomerise but is unable to insert into the membrane [10]. This produced traces similar to the disulfide-locked monomer mutant: thus the changes in the QCM-D signatures of both dsmSLO and ppSLO report lack of membrane insertion, rather than rearrangement and pre-pore formation. Subtle differences between monomer locked SLO and pre-pore locked SLO were highlighted when the first derivative was analysed. As discussed above this showed that ppSLO like wtSLO, displays two minima in $\Delta f'$ however the second event occurred earlier and likely represents oligomerisation without insertion. By contrast, dsmSLO lacked this second event. However the signature trace, $\Delta D'$ for ppSLO is similar to the dsmSLO trace, indicating that the lack of insertion results in the shift to the left for the second maximum.

In addition, on SiO_2 with eggPC:Chol these mutant SLOs bind but, unlike SLO or reduced dsmSLO, are easily washed off the lipid layer, suggesting that only inserted molecules are stably associated with the membrane. Therefore, using this experimental system we can apparently distinguish between binding/oligomerisation (steps 1 and 2) and insertion (step 3). However the molecular changes occurring between steps 1 and 2 do not produce detectable differences in either mass (Δf) or viscoelasticity (ΔD) (Fig. 6).

4.3. Pore formation

It is currently thought that before CDCs can penetrate membrane a complete ring structure (pre-pore) must be formed, which then triggers insertion [4]. Yet EM studies have consistently shown evidence of arcs [11,12,14,19–21,36]. Arcs are also apparent in a study by Czajkowsky and co-workers who used AFM to view another CDC, PFO [7]. They appear more frequently in images of wtPFO than in images of a disulfide trapped pre-pore locked mutant unable to unfurl transmembrane hairpin 1; this mutant shows predominantly full ring structures [7]. A simple explanation for the latter observation is that if insertion is prevented, partially completed pre-pores (containing fewer subunits) are more easily washed off the surface than completed pre-pores.

We also observed a high percentage of arcs on QCM-D sensors imaged by AFM. Many of these were intertwined and cannot easily be explained by breakage of completed rings, nor are they likely to be artefacts of the imaging process as it is much gentler compared to EM. In the conditions used for our AFM (SiO_2 with eggPC:Chol), mutants unable to insert into the lipid layer bind efficiently but wash off easily and essentially completely (Figs. 4F and 5F). Thus we suggest that the incomplete rings of wtSLO we see under AFM after washing are stably associated with the membrane via insertion, and hence completed pre-pore formation is not essential for insertion into the membrane. We do not suggest that oligomerisation and insertion is a coupled process, rather we suggest that insertion is possible after a threshold of subunit addition is reached but before ring formation is complete. Whether arcs are biologically active and occur in vivo, or represent failed and functionally irrelevant artefacts, are questions for future investigation, however earlier evidence suggests they are in fact functional [20].

4.4. Monitoring SLO pore formation by QCM-D

The traces obtained for Δf and ΔD are a similar shape over various concentrations, indicating that there is not a critical monomer concentration required for pore formation and insertion. Unlike the peptide maculatin [31] there is no evidence for decrease of mass from the surface of the sensor following initial binding, suggesting that lipids are not lost from the surface when SLO inserts and it is likely the lipid rearranges to accommodate the SLO pore. It is likely that the lipid bilayer corrugates to facilitate this. The shape of the curve for binding of SLO is identical over the various harmonics but the magnitude of the change in Δf is greatest in the harmonic that is furthest from the sensor surface (3rd), suggesting that there is more weight on the lipid compared to very close to the sensor's surface. This is consistent with the mode of SLO function, as the bulk of the protein remains above the membrane during and after pore formation. However we see very little difference in the spread of harmonics between SLO, dsmSLO and ppSLO, meaning that insertion of the ß strands into the bilayer does not produce changes that can be measured via different harmonics.

We were unable to investigate DMPC:Chol on SiO_2 due to the absence or inaccessibility of cholesterol in the final lipid layer (this was unexpected and limited our ability to directly compare Au–MPA and SiO_2). What this reflects in terms of membrane structure remains unclear. There are some small but clear differences in binding of wtSLO to eggPC:Chol membranes on Au–MPA versus SiO_2. This is demonstrated by the Δf–ΔD trace, where the overall shape of the trace is the same however the finer details differ. Differences between sensors were also evident when using the SLO mutants. On Au–MPA dsmSLO and ppSLO bind to the DMPC:Chol surface and do not easily wash off. On SiO_2 these mutants readily washed off the surface whereas wtSLO and reduced dsmSLO did not.

Collectively these observations indicate potential differences in the structure of lipid layers formed on Au–MPA vs SiO_2. It is possible that the surface roughness and/or MPA may force a different membrane structure compared to SiO_2. Alternatively, differences in the liquid crystal transition temperature (Tm) of DMPC and eggPC may impact the formation of a cholesterol-containing bilayer on SiO_2. The Tm is 24 °C for DMPC (just above the experimental temperature of 22 °C) and −15 °C for eggPC (well below). The addition of cholesterol can significantly affect the Tm, thus at 60% mol cholesterol differences in the fluid state of the membrane may directly affect overall membrane structure and hence SLO binding. The use of another complementary technique such as dual polarization interferometry, would may be helpful in identifying structural differences. This is an optical technique which provides simultaneous measurement of kinetic mass, thickness and birefringence. DPI has not been described for SLO but would be a very useful for providing information on the thickness of the bilayer.

5. Conclusion

In summary we have analysed membrane binding by SLO and monitored the changes in the lipid layer in real time using QCM-D. We have demonstrated that oligomerisation and pore formation occur on the sensors, thus providing new insight into pore formation by SLO. Binding mutants unable to form pores demonstrate that QCM-D can distinguish between binding and insertion through changes in dissipation. Contrary to the current model, our work suggests that partially completed, membrane-inserted pores can be formed by SLO.

Supplementary data to this article can be found online at http://dx.doi.org/10.1016/j.bbamem.2014.10.012.

Acknowledgements

We thank Prof. Bhakdi for providing the pMAL-SLO plasmid. This work was supported by grant 490900 to PIB from the National Health and Medical Research Council (Australia) and LLM and RFT from the Australian Research Council.

References

[1] E.M. Hotze, R.K. Tweten, Membrane assembly of the cholesterol-dependent cytolysin pore complex, Biochim. Biophys. Acta 1818 (2012) 1028–1038.
[2] A.J. Farrand, S. LaChapelle, E.M. Hotze, A.E. Johnson, R.K. Tweten, Only two amino acids are essential for cytolytic toxin recognition of cholesterol at the membrane surface, Proc. Natl. Acad. Sci. 107 (2010) 4341–4346.
[3] Y. Ohno-Iwashita, M. Iwamoto, K. Mitsui, S. Ando, S. Iwashita, A cytolysin, theta-toxin, preferentially binds to membrane cholesterol surrounded by phospholipids with 18-carbon hydrocarbon chains in cholesterol-rich region, J. Biochem. 110 (1991) 369–375.
[4] E.M. Hotze, E. Wilson-Kubalek, A.J. Farrand, L. Bentsen, M.W. Parker, A.E. Johnson, R.K. Tweten, Monomer–monomer interactions propagate structural transitions necessary for pore formation by the cholesterol-dependent cytolysins, J. Biol. Chem. 287 (2012) 24534–24543.
[5] M. Palmer, I. Vulicevic, P. Saweljew, A. Valeva, M. Kehoe, S. Bhakdi, Streptolysin O: a proposed model of allosteric interaction between a pore-forming protein and its target lipid bilayer†, Biochemistry 37 (1998) 2378–2383.
[6] E.M. Abdel Ghani, S. Weis, I. Walev, M. Kehoe, S. Bhakdi, M. Palmer, Streptolysin O: inhibition of the conformational change during membrane binding of the monomer prevents oligomerization and pore formation†, Biochemistry 38 (1999) 15204–15211.
[7] D.M. Czajkowsky, E.M. Hotze, Z. Shao, R.K. Tweten, Vertical collapse of a cytolysin prepore moves its transmembrane beta-hairpins to the membrane, EMBO J. 23 (2004) 3206–3215.
[8] L.A. Shepard, O. Shatursky, A.E. Johnson, R.K. Tweten, The mechanism of pore assembly for a cholesterol-dependent cytolysin: formation of a large prepore complex precedes the insertion of the transmembrane beta-hairpins, Biochemistry 39 (2000) 10284–10293.
[9] E.M. Hotze, E.M. Wilson-Kubalek, J. Rossjohn, M.W. Parker, A.E. Johnson, R.K. Tweten, Arresting pore formation of a cholesterol-dependent cytolysin by disulfide trapping synchronizes the insertion of the transmembrane beta-sheet from a prepore intermediate, J. Biol. Chem. 276 (2001) 8261–8268.
[10] N. Magassa, S. Chandrasekaran, M.G. Caparon, Streptococcus pyogenes cytolysin-mediated translocation does not require pore formation by streptolysin O, EMBO Rep. 11 (2010) 400–405.
[11] S. Bhakdi, J. Tranum-Jensen, A. Sziegoleit, Mechanism of membrane damage by streptolysin-O, Infect. Immun. 47 (1985) 52–60.
[12] K. Sekiya, H. Danbara, Y. Futaesaku, [Mechanism of pore formation on erythrocyte membrane by streptolysin-O], Kansenshogaku Zasshi 67 (1993) 736–740.
[13] M. Walch, U. Ziegler, P. Groscurth, Effect of streptolysin O on the microelasticity of human platelets analyzed by atomic force microscopy, Ultramicroscopy 82 (2000) 259–267.
[14] W. Niedermeyer, Interaction of streptolysin-O with biomembranes: kinetic and morphological studies on erythrocyte membranes, Toxicon 23 (1985) 425–439.
[15] I. Walev, S.C. Bhakdi, F. Hofmann, N. Djonder, A. Valeva, K. Aktories, S. Bhakdi, Delivery of proteins into living cells by reversible membrane permeabilization with streptolysin-O, Proc. Natl. Acad. Sci. U. S. A. 98 (2001) 3185–3190.
[16] S. Bhakdi, U. Weller, I. Walev, E. Martin, D. Jonas, M. Palmer, A guide to the use of pore-forming toxins for controlled permeabilization of cell membranes, Med. Microbiol. Immunol. 182 (1993) 167–175.
[17] T. Wilkop, D. Xu, Q. Cheng, Characterization of pore formation by streptolysin O on supported lipid membranes by impedance spectroscopy and surface plasmon resonance spectroscopy, Langmuir 23 (2007) 1403–1409.
[18] H. Helmholz, Selective toxin-lipid membrane interactions of natural, haemolytic Scyphozoan toxins analyzed by surface plasmon resonance, Biochim. Biophys. Acta 1798 (2010) 1944–1952.
[19] J.R. Harris, M. Adrian, S. Bhakdi, M. Palmer, Cholesterol–streptolysin O interaction: an em study of wild-type and mutant streptolysin O, J. Struct. Biol. 121 (1998) 343–355.
[20] M. Palmer, R. Harris, C. Freytag, M. Kehoe, J. Tranum-Jensen, S. Bhakdi, Assembly mechanism of the oligomeric streptolysin O pore: the early membrane lesion is lined by a free edge of the lipid membrane and is extended gradually during oligomerization, EMBO J. 17 (1998) 1598–1605.
[21] U. Weller, L. Muller, M. Messner, M. Palmer, A. Valeva, J. Tranum-Jensen, P. Agrawal, C. Biermann, A. Dobereiner, M.A. Kehoe, S. Bhakdi, Expression of active streptolysin O in *Escherichia coli* as a maltose-binding-protein–streptolysin-O fusion protein. The N-terminal 70 amino acids are not required for hemolytic activity, Eur. J. Biochem. 236 (1996) 34–39.
[22] M. Palmer, A. Valeva, M. Kehoe, S. Bhakdi, Kinetics of streptolysin O self-assembly, Eur. J. Biochem. 231 (1995) 388–395.
[23] S.E. Stewart, S.C. Kondos, A.Y. Matthews, M.E. D'Angelo, M.A. Dunstone, J.C. Whisstock, J.A. Trapani, P.I. Bird, The perforin pore facilitates the delivery of cationic cargos, J. Biol. Chem. 289 (2014) 9172–9181.
[24] S. Piantavigna, G.A. McCubbin, S. Boehnke, B. Graham, L. Spiccia, L.L. Martin, A mechanistic investigation of cell-penetrating Tat peptides with supported lipid membranes, Biochim. Biophys. Acta 1808 (2011) 1811–1817.
[25] A. Mechler, S. Praporski, S. Piantavigna, S.M. Heaton, K.N. Hall, M.I. Aguilar, L.L. Martin, Structure and homogeneity of pseudo-physiological phospholipid bilayers and their deposition characteristics on carboxylic acid terminated self-assembled monolayers, Biomaterials 30 (2009) 682–689.
[26] G. Sauerbrey, Verwendung von Schwingquarzen zur Wägung dünner Schichten und zur Mikrowägung, Z. Phys. 155 (1959) 206–222.
[27] R.F. Tabor, J. Eastoe, P.J. Dowding, A two-step model for surfactant adsorption at solid surfaces, J. Colloid Interface Sci. 346 (2010) 424–428.
[28] L.H. Torn, L.K. Koopal, A. de Keizer, J. Lyklema, Adsorption of nonionic surfactants on cellulose surfaces: adsorbed amounts and kinetics, Langmuir 21 (2005) 7768–7775.
[29] G.A. McCubbin, S. Praporski, S. Piantavigna, D. Knappe, R. Hoffmann, J.H. Bowie, F. Separovic, L.L. Martin, QCM-D fingerprinting of membrane-active peptides, Eur. Biophys. J. 40 (2011) 437–446.
[30] R. Ramachandran, R.K. Tweten, A.E. Johnson, Membrane-dependent conformational changes initiate cholesterol-dependent cytolysin oligomerization and intersubunit beta-strand alignment, Nat. Struct. Mol. Biol. 11 (2004) 697–705.
[31] A. Mechler, S. Praporski, K. Atmuri, M. Boland, F. Separovic, L.L. Martin, Specific and selective peptide–membrane interactions revealed using quartz crystal microbalance, Biophys. J. 93 (2007) 3907–3916.
[32] A.P. Heuck, E.M. Hotze, R.K. Tweten, A.E. Johnson, Mechanism of membrane insertion of a multimeric beta-barrel protein: perfringolysin O creates a pore using ordered and coupled conformational changes, Mol. Cell 6 (2000) 1233–1242.
[33] J.J. Flanagan, R.K. Tweten, A.E. Johnson, A.P. Heuck, Cholesterol exposure at the membrane surface is necessary and sufficient to trigger perfringolysin O binding, Biochemistry 48 (2009) 3977–3987.
[34] T. Wilkop, D. Xu, Q. Cheng, Electrochemical characterization of pore formation by bacterial protein toxins on hybrid supported membranes, Langmuir 24 (2008) 5615–5621.
[35] F. Hugo, J. Reichwein, M. Arvand, S. Kramer, S. Bhakdi, Use of a monoclonal antibody to determine the mode of transmembrane pore formation by streptolysin O, Infect. Immun. 54 (1986) 641–645.
[36] R.J. Gilbert, Inactivation and activity of cholesterol-dependent cytolysins: what structural studies tell us, Structure 13 (2005) 1097–1106.